Applied Catalysis A: General 450 (2013) 34–41

Contents lists available at SciVerse ScienceDirect

Applied Catalysis A: General

journal homepage: www.elsevier.com/locate/apcata

Sulfonic acid functionalized MCM-41 as solid acid catalyst for *tert*-butylation of hydroquinone enhanced by microwave heating

Eng-Poh Ng[a,*], Siti Norbayu Mohd Subari[a], Olivier Marie[b], Rino R. Mukti[c], Joon-Ching Juan[d]

[a] School of Chemical Sciences, Universiti Sains Malaysia, 11800 USM Penang, Malaysia
[b] Laboratoire Catalyse & Spectrochimie, ENSICAEN, Université de Caen, 14000 Caen, France
[c] Division of Inorganic and Physical Chemistry, Institut Teknologi Bandung, Jl Ganesha no. 10, Bandung 40132, West Java, Indonesia
[d] Laboratory of Applied Catalysis and Environmental Technology, School of Science, Monash University, Bandar Sunway 46150, Malaysia

ARTICLE INFO

Article history:
Received 25 July 2012
Received in revised form
12 September 2012
Accepted 30 September 2012
Available online 3 November 2012

Keywords:
Mesoporous material
Sulfonation
Sulfonic acid
tert-Butylation
Microwave synthesis

ABSTRACT

Covalently linked sulfonic acid (—SO_3H) modified MCM-41 mesoporous catalysts was prepared, characterized and its catalytic activity under microwave irradiation was evaluated. The NH_2-MCM-41 was first prepared by anchoring (3-aminopropyl)triethoxysilane (APTES) on Si-MCM-41 and further reacted with 1,4-butane-sultone to yield the desired acid catalyst. The mesophase and porosity of samples were determined by XRD, TEM and N_2 sorption isotherm analyses. The presence of sulfonic acid moiety was confirmed by FT-IR, TG/DTA, sulfur elemental analysis and in situ IR study of pyridine and ammonia adsorptions. The catalyst showed high catalytic activity and high selectivity in *tert*-butylation of hydroquinone under microwave irradiation. No leaching problem was observed after several runs, while the catalyst can be recovered and reused without loss of reactivity under the described reaction conditions.

1. Introduction

New developments in the chemical industries are driven by environmental regulations, safety, energy efficiencies and the need for improved performance. The increasingly environmental regulations require the use of green technology in various areas [1,2]. Particularly, catalysts are attractive in green technology because of their importance in petrochemicals and fine chemicals synthesis. Usually chemical syntheses involve homogeneous catalysts; however, using heterogeneous catalysts such as molecular sieves (e.g. microporous zeolites and mesoporous materials) could be more environment-friendly and cost effective, allowing catalyst separation and reusability [3].

MCM-41 is a structurally well-ordered mesoporous solid, possessing some fascinating properties such as high surface area, uniform pore size (20–100 Å) and relatively hydrophobic nature [4]. It is known that MCM-41 in pure silica form has no substantial acidity and exhibits only weak hydrogen bonding sites [5,6]. The incorporation of metals (Al, Ti, Fe, etc.) in MCM-41 framework structure can be performed to generate acid properties [7–10]. On the other side, functionalizing and supporting some acidic species such as heteropolyacids (HPW) [11–13] and mineral acids (H_3PO_4, H_2SO_4) [14–16] offer another promising solutions to generate the acidity.

Recently, MCM-41 grafted with sulfonic acid (SO_3H-MCM-41) has been prepared to catalyze many organic reactions. The modified catalyst improves the solid acidity and at the same time, high surface areas and tunable pore diameters are retained. For instance, SO_3H-MCM-41 is shown having excellent catalytic activity and selectivity in esterification [17–22], Fischer indole synthesis [23], Claisen–Schmidt condensation [24], Friedel–Crafts alkylation [25,26], Fries and pinacol rearrangements [26], condensation of 2-methylfuran and acetone [27] and transesterification reactions [28]. The results reveal that incorporation of sulfonic acid groups on porous silica supports produces highly convenient solid acid catalysts, exhibiting the advantages of homogeneous catalysts.

Basically, covalent anchoring of the sulfonic acid groups to the mesoporous materials surface can be achieved either by a direct synthesis route or by a post synthetic anchoring of 3-(mercaptopropyl)triethoxysilane (MPTES) followed by an oxidation step to generate the sulfonic acid groups [17–22,28–30]. However, the use of strong oxidation agent in the oxidization of MPTES tends to lower the ordering of the mesopores. In respect to this, chlorosulfonic acid has recently been proposed as another

* Corresponding author. Tel.: +60 4 653 4021.
E-mail address: epng@usm.my (E.-P. Ng).

0926-860X/$ – see front matter © 2012 Elsevier B.V. All rights reserved.
http://dx.doi.org/10.1016/j.apcata.2012.09.055

promising sulfonating agent to immobilize sulfonic acid groups on mesopore walls [22,26].

Alkylsultones are cyclic sulfate esters. Basically, they are used as main chemical intermediates for the synthesis of dyes, anionic surfactants and secondary lithium ion solution [31]. In this work, the use of alkylsultone was achieved to generate sulfonic acid groups on MCM-41 solid via ring opening approach in an attempt to obtain a heterogeneous acid catalyst. The mesoporous silica was first aminopropylated followed by sulfonation with alkylsultone. The resulting solids were then characterized and their catalytic activity was studied using microwave-assisted Friedel–Crafts *tert*-butylation of hydroquinone as the probe reaction. This reaction was interesting as it can predict the nature of the acidic sites (weak, mild or strong) present in the catalysts [32,33] which will be further confirmed by in situ IR study of pyridine and ammonia adsorptions study. Furthermore, the monosubstituted product of this reaction namely, 2-*tert*-butylhydroquinone, is a highly effective antioxidant and is widely used as a preservative for vegetable oils and edible animal fats [34,35].

2. Experimental

2.1. Preparation of Si-MCM-41 support

The mesoporous MCM-41 powder was synthesized from an alkaline solution containing cetyltrimethylammonium bromide (CTABr, 98%, Aldrich), sodium silicate solution (Na_2O 7.5–8.5%, SiO_2 25.8–28.5%, Merck), sulfuric acid (98%, Merck), and deionized water. CTABr was first dissolved in distilled water under stirring before sodium silicate was introduced into the mixture to give the final composition mole ratio of $1CTABr:1.76Na_2O:6.14SiO_2:335.23H_2O$. After 24 h of hydrothermal treatment at 100 °C, the MCM-41 powder was filtered, washed until pH 7, and dried at 80 °C overnight before it was calcined in a furnace under a flow of air at 550 °C for 4 h with a heating rate of 1 °C/min to remove the organic template.

2.2. Preparation of (3-aminopropyl)triethylsilyl-MCM-41 (NH_2-MCM-41) via aminopropylation

Amine functionalization was achieved by aminopropylating activated Si-MCM-41 (1.5 g, 100 °C, 4 h, Fig. 1a) under vacuum with (3-aminopropyl)triethoxysilane (3.5 g, APTES, 98%, Aldrich) in toluene (10 ml) under reflux for 5 h to form covalent linkages with the mesoporous silica surface (Fig. 1b). The non-reacted amines and the solvent were removed by filtration and the amine modified MCM-41 was washed thoroughly with chloroform and diethyl ether before drying at 80 °C overnight.

2.3. Preparation of SO_3H-MCM-41 via sulfonation

The NH_2-MCM-41 (1.0 g) was preloaded with a solution of toluene (10 ml) containing 1,4-butane-sultone (3 g, Merck) followed by reflux for 5 h. The solid obtained was then purified with chloroform and diethyl ether before drying at 80 °C overnight to give a yellow powder as final product (Fig. 1c).

2.4. Characterization of catalysts

XRD patterns were recorded on a Siemens D5000 Kristalloflex diffractometer. The surface physicochemical properties were analyzed using a Micromeritics ASAP 2010 after degassing overnight at 180 °C. The morphological features of MCM-41 samples were examined by transmission electron microscopy (TEM) using PHILIPS CM-12 microscope. For the quantitative determination of sulfur content or SO_3H density in the samples, the MCM-41 solids were measured with a KZDL-4 Sulfur Analyzer. The organic moieties were determined based on Mettler TGA SDTA851 instrument with a heating rate of 10 °C/min under nitrogen flow. The FTIR spectra were recorded on a PerkinElmer spectrometer (System 2000) using the KBr pellet technique (KBr: sample weight ratio = 150:1).

Pyridine and ammonia FTIR spectra were recorded using a Nicolet 6700 FT-IR spectrometer. The MCM-41 samples were ground and pressed to obtain a wafer (area 2 cm^2, mass of 13 mg) before introduction in the IR cell. The samples were then pre-activated under vacuum (10^{-6} mbar) at 200 °C for 3 h. The reference spectrum was first recorded after cooling and then a 1.33 mbar equilibrium pressure of pyridine (or ammonia) was introduced to the sample for 5 min. The spectrum was recorded with a 4 cm^{-1} resolution and 64 scans accumulation. The sample was then allowed to evacuate at 25 and 100 °C to desorb pyridine (or ammonia) and the spectra were recorded after each evacuation step.

2.5. Catalytic experiments

Friedel–Crafts reactions were performed with microwave irradiation assistance by modifying the synthesis condition [30]. Prior to reaction, hydroquinone (Merck, 2.0 mmol), methyl *tert*-butyl ether (MTBE, Merck, 2.0 mmol) and freshly activated SO_3H-MCM-41 catalyst (0.1 g, 100 °C, 3 h) were loaded into a reactor. The reaction was realized in an Anton Paar Synthos 3000 microwave oven under magnetic stirring and 300 W microwave irradiation, while the reaction temperature was monitored by an infrared pyrometer. The samples were withdrawn after the reaction and the liquid phase was separated and analyzed using a gas chromatograph (Hewlett-Packard 5880) equipped with a Carbowax Equity 1 non-polar capillary column. The identity of the product was confirmed by GC–MS (Perkin-Elmer GC-IR 2000 system).

2.6. Leaching and reusability tests

The leaching and reusability tests were carried out as follows: SO_3H-MCM-41 solid was separated after the first Friedel–Crafts (reaction temperature = 150 °C, HQ:MTBE = 1:1, MW power = 300 W, time = 8 min) run, further washed with diethyl ether and finally activated (100 °C, 3 h) before use for the three subsequent cycles of catalytic reaction. After the reaction, the solution was again separated and analyzed using GC.

3. Results and discussion

3.1. Characterization

Supported sulfonic acid catalysts in this work were prepared in two steps. In the initial step, APTES as a bridging agent was first functionalized on MCM-41, giving (3-aminopropyl)trimethylsilyl-MCM-41 (denoted as NH_2-MCM-41). After this, the nucleophilic attack of the amine group of NH_2-MCM-41 on the cyclic sultone opened the ring of 1,4-butane-sultone, leading to the formation of a linear chain of sulfonic acid solid catalyst (Fig. 1c).

The preparation of SO_3H-MCM-41 was monitored using FT-IR spectroscopy via the KBr salt dilution technique. Fig. 2 shows the infrared spectra of Si-MCM-41, NH_2-MCM-41, and SO_3H-MCM-41 solids. The spectrum shown in Fig. 2a displays several typical IR vibration signals for Si-MCM-41: 3455 and 1642 cm^{-1} (H-bonded hydroxyls ν(OH) stretching and adsorbed water bending vibrations), 1237 and 1085 cm^{-1} (asymmetric stretching vibrations of Si–O–Si), 800 and 584 cm^{-1} (symmetric stretching vibrations of Si–O–Si), 962 cm^{-1} (bending mode of Si–OH) and 464 cm^{-1} (bending vibration of Si–O–Si) [15]. After aminopropylation, the band at 962 cm^{-1} almost completely disappeared and several new vibration bands including those corresponding to C–H groups (2934,

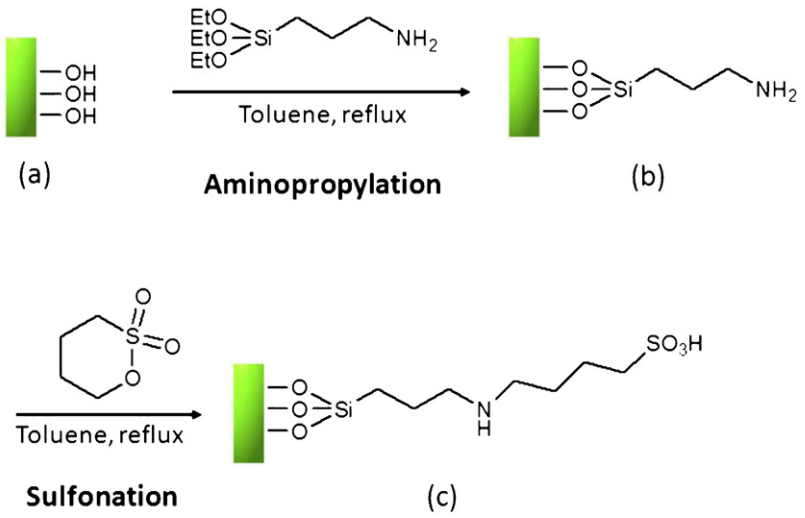

Fig. 1. Anchoring of sulfonic acid functional groups on MCM-41 support.

2854 cm^{-1}) emerged, showing that the APTES has been successfully reacted with surface silanol groups and covalently attached to the MCM-41 (Fig. 2b). In addition, the appearance of two N–H stretching vibrations at 3560 and 3491 cm^{-1}, and two N–H bending vibrations at 1623 and 1569 cm^{-1} can also be considered as an evidence for the presence of APTES on the surface of the grafted materials [36]. These four peaks, however, completely vanished upon the sulfonation treatment (Fig. 2c).

The existence of sulfonic acid group (—SO_3H) in the samples was further confirmed by the presence of an intense and broad absorption band at 3428 cm^{-1} which corresponds to S–OH stretching vibration, and the most intense signals at 1160 and 1080 cm^{-1} which refers to the asymmetric vibration of S=O and symmetric stretching vibration of SO_3H group, respectively [37]. In addition, two vibration bands at 1220 and 1348 cm^{-1}, respectively assign to the symmetric and asymmetric SO_2 stretching modes were also observed [38]. Thus, all these results reveal that the ring opening of 1,4-butane-sultone occurred and the sulfonic acid functional group was successfully anchored on the walls of MCM-41.

The species providing active sites in SO_3H-MCM-41 was further investigated using infrared spectroscopy. It is known that the use of cyclic sultone in the present organic synthesis tends to give ammonium sulfate as the product [39]. In order to confirm whether the active site of SO_3H-MCM-41 is ammonium sulfonate or sulfonic acid bound to APTES, a careful investigation of the N–H bending vibration peaks was performed. From the infrared spectrum in Fig. 2c, the vibration band corresponding to the N–H bending modes of alkyl ammonium cation at 1487 and 1464 cm^{-1} were not observed and thus excluding the existence of ammonium sulfonate in SO_3H-MCM-41 [40]. Instead, two IR bands were detected at 1545 and 1469 cm^{-1} which can be assigned to the bending vibration of primary amine [41]. Thus, the IR spectroscopy suggested that the active site of SO_3H-MCM-41 rather originates from sulfonic acid bound to amine group.

The ordered mesoporosity of MCM-41 solids was determined by XRD analysis. The XRD pattern of calcined Si-MCM-41 exhibits an intense signal at $2\theta = 2.2^\circ$ corresponding to (1 0 0) plane and three small signals between 3.5° and 6.0° due to (1 1 0), (2 0 0) and (2 1 0) planes which confirms the presence of well-defined hexagonal MCM-41 (Fig. 3a) [4]. As aminopropylation and sulfonation modifications took place, the signals shifted toward higher diffraction angles (Fig. 3b, c). This shift can be explained by a slight decrease in the pore size resulting from the insertion of APTES and linear sulfonic acid into the MCM-41 pores [42]. In addition, less intense and broadened diffraction peaks were also observed for both NH_2-MCM-41 and SO_3H-MCM-41, showing that the structural integrity in MCM-41 was slightly degraded upon surface modification. Nevertheless, the characteristic diffraction peaks of both samples were

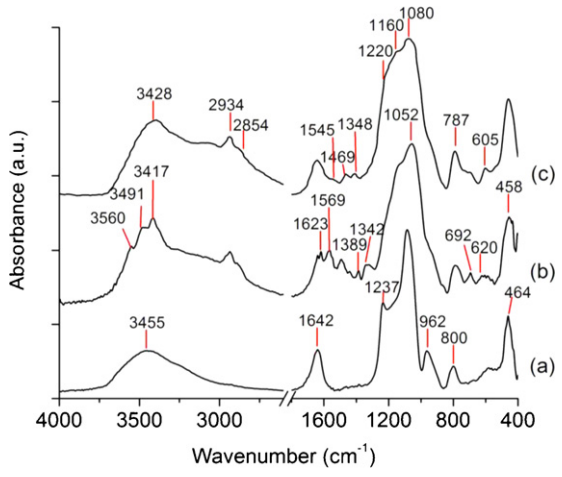

Fig. 2. KBr diluted IR spectra of (a) Si-MCM-41, (b) NH_2-MCM-41, and (c) SO_3H-MCM-41.

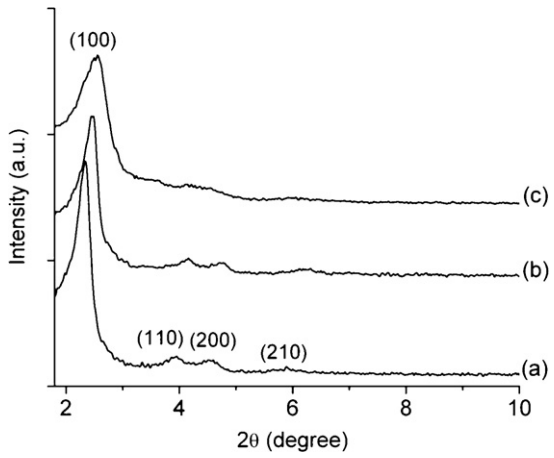

Fig. 3. XRD patterns of (a) Si-MCM-41, (b) NH_2-MCM-41, and (c) SO_3H-MCM-41.

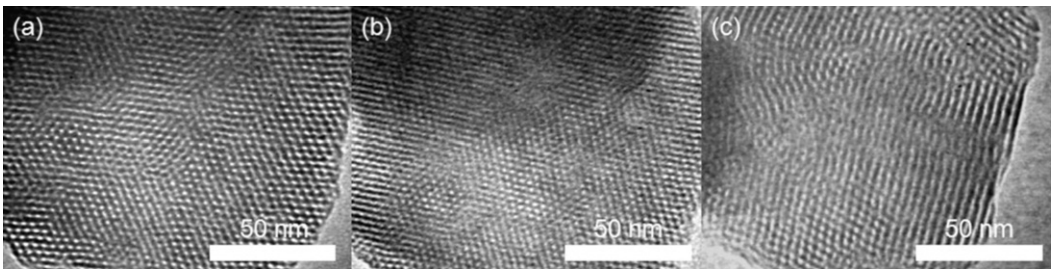

Fig. 4. TEM images of (a) Si-MCM-41, (b) NH_2-MCM-41, and (c) SO_3H-MCM-41.

retained indicating that the long-range order of mesoporous hexagonal channels was still preserved after modification.

The XRD results were further confirmed by TEM analysis. The hexagonal periodicity of the mesophase of Si-MCM-41 and NH_2-MCM-41 was basically maintained, as displayed in the TEM images (Fig. 4a, b). However, the channels in SO_3H-MCM-41 partially collapsed, in some degree, into disordered and wormhole-like packings (Fig. 4c). These observations are fully in line with the XRD data.

The SO_3H density of SO_3H-MCM-41 was then investigated with sulfur elemental analysis. No sulfur element was detected in both Si-MCM-41 and NH_2-MCM-41. After sulfonation modification and proper washing, the SO_3H-MCM-41 sample contained 2.069% of sulfur or equivalent to 0.647 mmol/g of sulfur or SO_3H group.

The existence of APTES and linear butyl sulfonic acid was further proven based on TG/DTA and sulfur analyses. In Fig. 5, the TG/DTA-curves of MCM-41 samples are given. A one-step weight loss at 150 °C was observed for Si-MCM-41 which is due to water desorption (Fig. 5a). After aminopropylation, two additional weight losses appeared at 150–350 °C (3.5 wt.%) and 350–650 °C (18.4 wt.%) with an endothermic DTA signal at 500 °C, showing that the APTES has been successfully functionalized onto MCM-41 surface (Fig. 5b). This APTES group was strongly bonded to the MCM-41 via covalent bonding and did not easily detach from the siloxane surface under mild functionalization condition (e.g. 110 °C, 5 h) [43,44]. For SO_3H-MCM-41, three weight loss stages were detected, but the TGA curve pattern was totally different from that of the NH_2-MCM-41 (Fig. 5c). Furthermore, an additional strong and sharp endothermic DTA signal was observed at 400 °C which could be due to the decomposition of sulfonic acid compound [45] (inset of Fig. 5c). The differences of TG/DTA profiles between NH_2-MCM-41 and SO_3H-MCM-41 agree with the IR spectroscopy results and clearly evidence the successful anchoring of sulfonic acid group on the MCM-41 surface.

The textural properties of Si-MCM-41, NH_2-MCM-41 and SO_3H-MCM-41 were further investigated using N_2 sorption analysis. All solids exhibited type IV isotherms with H1 hysteresis loops [46] (Fig. 6). Upon functionalization of the parent material with APTES and linear butyl sulfonic acid, changes in the N_2 sorption isotherm curves and consequently decreases in the gas uptake were observed. This could be attributed to the attachment and occupation of organic molecules onto the surface of the inner pores (Fig. 6; Table 1). Interestingly, a shrinkage in the pore diameter from the initial value of 2.60 nm (Si-MCM-41) to 1.28 nm (SO_3H-MCM-41) was also observed and confirmed the presence of sulfonic acid compounds on the parent MCM-41 (Fig. 6; Table 1).

The presence of acid sites on the surface of the SO_3H-MCM-41 catalyst was investigated with pyridine and ammonia adsorptions monitored by FT-IR spectroscopy. The pyridine and ammonia adsorptions were performed at room temperature and followed by evacuation at increasing temperatures. The positions and intensities of the IR bands were then monitored. It is worth noting that bands pre-existing on the bare sample may shift upon interaction with adsorbed species. Consequently, a preliminary look at the spectrum obtained after the thermal activation of SO_3H-MCM-41 at 200 °C under a vacuum (Fig. 7a) appears necessary. At such a temperature, the TG analysis (Fig. 5) showed that most of the adsorbed water is removed and this may explain the shift of certain bands ($1645 \rightarrow 1655\ cm^{-1}$ and $1348 \rightarrow 1410\ cm^{-1}$) when compared with their position observed with the KBr salt dilution method (Fig. 2) for which the powder was characterized in the hydrated state. More precisely, the detailed analysis of the 1700–1400 cm^{-1} region reveals the presence of a broad band at 1535 cm^{-1} and a doublet at 1469–1446 cm^{-1}. The former band possibly is attributed to the partially substituted APTES, while the two later would stand for distinct δ(CH) bending modes of APTES and butyl sulfonic acid.

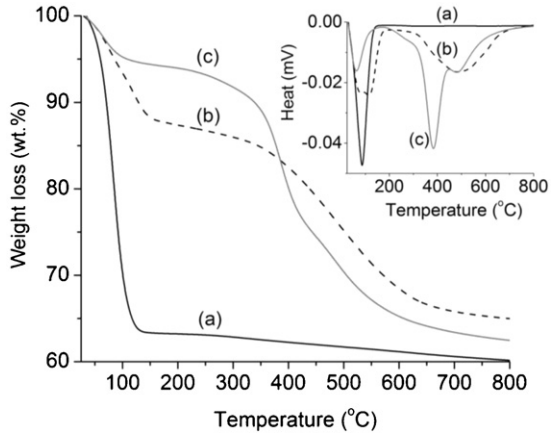

Fig. 5. TG curves of (a) Si-MCM-41, (b) NH_2-MCM-41, and (c) SO_3H-MCM-41. Inset: DTA curves of (a) Si-MCM-41, (b) NH_2-MCM-41, and (c) SO_3H-MCM-41.

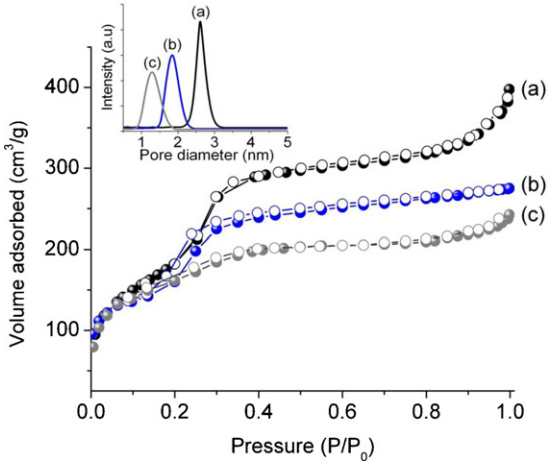

Fig. 6. Nitrogen adsorption (closed symbol) and desorption (open symbol) isotherms of (a) Si-MCM-41, (b) NH_2-MCM-41 and (c) SO_3H-MCM-41. Inset: Pore size distributions derived from nitrogen adsorption analysis.

Table 1
Textural properties of the MCM-41 samples.

Samples	d_{100} spacing (nm)	Unit cell, a_0 (nm)[a]	Pore size (nm)[b]	Surface area, S_{BET} (m^2/g)	Pore volume, V_{total} (cm^3/g)
Si-MCM-41	4.42	51.12	2.60	938	0.61
NH_2-MCM-41	4.31	49.71	1.81	508	0.43
SO_3H-MCM-41	4.16	48.02	1.28	475	0.38

[a] $a_0 = 2d_{100}/\sqrt{3}$.
[b] Average pore diameter by BJH.

However, the broadness of the later bands could also indicate the presence of an intramolecular H-bond between the SO_3H and the NH groups (Fig. 7, inset without the Py molecule). Upon pyridine introduction at 25 °C, new bands emerge as reported in Fig. 7b. The interaction of pyridine via the nitrogen lone-pair electrons, with aprotic (Lewis) and protonic (Brönsted) acid sites, can be detected by monitoring the ring vibration modes 8a, 8b, 19a, and 19b, named according to the nomenclature introduced by Wilson [47]. These modes, which appear at 1598 cm^{-1} (8a), 1580 cm^{-1} (8b), 1483 cm^{-1} (19a), and 1437 cm^{-1} (19b) in the IR spectrum of liquid pyridine, undergo upward frequency shifts upon coordination of the probe molecule to either type of acid sites. The Brönsted acidity which is expected in the present case can be tested by the formation of pyridinium (PyH^+) species, characterized by the bands at about 1640 and 1545 cm^{-1} [48–50]. Here, the main new bands at 1595, 1580, 1478, 1444 and 1437 cm^{-1} reveal physisorbed pyridine molecules together with Py species linked to acidic surface groups through H-bonding. For sure, the bands at 1547 and 1640 cm^{-1} are also detected, but several data allow excluding the hypothesis they characterize PyH^+ species. First, the intrinsic shape of the 1547 cm^{-1} component (FWHM = 40 cm^{-1}) observed upon interaction of pyridine with SO_3H-MCM-41 does not match with that expected for PyH^+. Fig. 7e indeed represents, for comparison purpose, the typical spectrum obtained after pyridine protonation upon interaction with an acidic H-MOR zeolite. In that case, the 1544 cm^{-1} component is much sharper (FWHM = 10 cm^{-1}). Secondly, the 1595:1547 cm^{-1} band intensity ratio does not match neither. Finally, no band typical for physisorbed Py species is expected below 1420 cm^{-1}, while a rather intense and broad band is detected at 1410 cm^{-1} upon interaction with SO_3H-MCM-41. As such a band already exists on the bare support with a much higher intensity (reference spectrum Fig. 7a was divided by a factor 40), one may suggest that it characterizes an intrinsic vibration of the catalyst perturbed by neighboring species, i.e. the higher the amount of perturbing species (upon adsorption), the higher the band intensity (inset of Fig. 7 illustrates the situation when a proton form the sulfonic group is shared between three bases: SO_3^-, R_1R_2NH and Py). A similar explanation would be valid for the increasing broad bands at 1655 and 1547 cm^{-1} (accompanied by an upward shift for the later one 1535 → 1547 cm^{-1}).

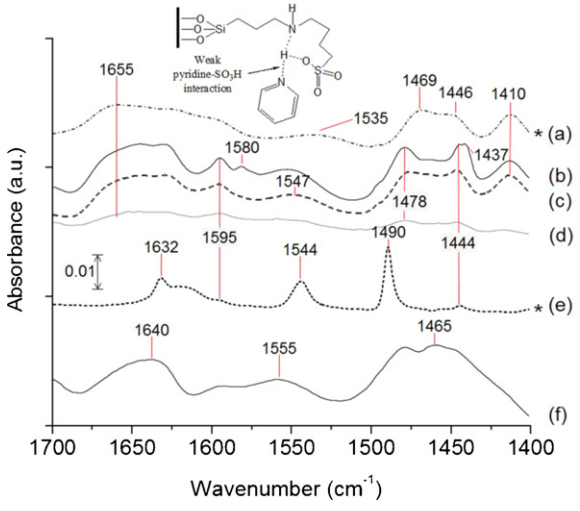

Fig. 7. FTIR spectra of SO_3H-MCM-41. (a) After thermal activation under a vacuum at 200 °C (used as the reference spectrum), (b) after pyridine adsorption at 25 °C (1.33 mbar at equilibrium for 5 min), (c) followed by evacuation at 25 °C, (d) evacuation at 100 °C, (e) IR spectrum relative to pyridine adsorption over H-MOR for comparison purpose and (f) IR spectrum relative to ammonia adsorption over SO_3H-MCM-41 at 25 °C (1.33 mbar for 5 min). Spectra labeled with (*) were multiplied by 0.025 and spectra (b), (c), (d) and (f) are corrected from the (a) reference spectrum. Inset: Possible way of interaction between pyridine and Brönsted acid site of SO_3H-MCM-41 catalyst perturbed by neighboring species.

After an evacuation at 25 °C consecutive to the Py adsorption, the bands at 1580 and 1437 cm^{-1} completely vanished (Fig. 7c) which confirm their assignment to physisorbed (pseudo liquid) species. On the contrary, bands at 1595, 1478 and 1444 cm^{-1} resist to a similar evacuation and measurable intensities even remain after an evacuation at 100 °C (Fig. 7d). These three later bands are thus assigned to pyridine interacting via H-bond with weak to mild Brönsted acidic sites from the SO_3H-MCM-41 catalyst (inset of Fig. 7). In order to confirm the presence of weak Brönsted acidic sites, ammonia, which is a harder and more basic probe molecule, was also adsorbed. The resulting spectrum (Fig. 7f) clearly illustrates the appearance of two broad multi-component bands centered at 1465 and 1640 cm^{-1} which can confidently be assigned to the δa(N–H) and δs(N–H) bending modes of the NH_4^+ species [51]. The proton transfer from the acidic SO_3H-MCM-41 to the more basic ammonia then effectively proceeds [as confirmed by the appearance of corresponding ν(N–H) stretching bands (not shown)]. Thus, the whole presented results reveal that Brönsted acidity exists in the SO_3H-MCM-41 and that the corresponding strength ranges from weak to mild.

3.2. Catalytic study

3.2.1. Effect of catalyst and reaction time

SO_3H-MCM-41 solid was applied as catalyst for *tert*-butylation of hydroquinone at 150 °C under microwave irradiation. In the absence of SO_3H-MCM-41 catalyst, the conversion rate of *tert*-butylation was slow and small conversion (<8%) was observed after 8 min of microwave treatment, showing that microwaves were catalytically inactive. When SO_3H-MCM-41 was introduced into the reactant mixture, a remarkable catalytic activity was observed. The high catalytic performance of SO_3H-MCM-41 was clearly demonstrated since a high hydroquinone conversion (88.0%) with a high selectivity (93.1%) to 2-*tert*-butylhydroquinone (2-TBHQ) was achieved after 8 min (Fig. 8A, B). In addition, only small quantity of 2,6-di-*tert*-butylhydroquinone (2,6-DTBHQ, 4.0%) and other byproducts (2.9%) was observed in the reaction. This result reveals that a molecular sieving effect takes place in the internal mesopores of the catalyst, which favors only the formation of monosubstituted *tert*-butyl product. At the same time, the formation of di-*tert*-butylated product was successfully restricted which should be also associated with the use of a low MTBE concentration during alkylation reaction and the use of weak to mild acidic SO_3H-MCM-41 catalyst. According to Ng et al. [16], mono-alkylated product is highly favored in Friedel–Crafts alkylation reaction especially in

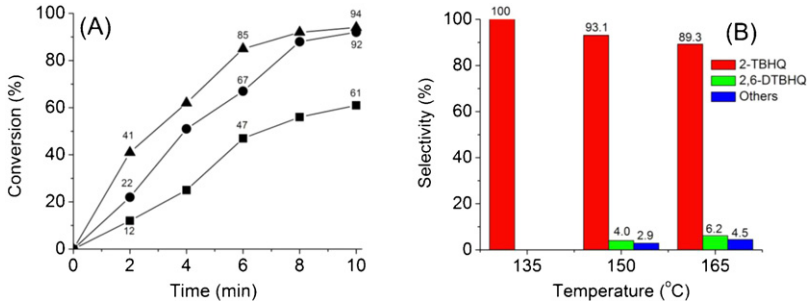

Fig. 8. (A) Conversion of hydroquinone at 135 °C (squares), 150 °C (circles) and 165 °C (triangles) using SO_3H-MCM-41 as catalyst. (B) Effect of temperature on the selectivity of *tert*-butylated products. Catalyst = 0.1 g, HQ:MTBE = 1:1, solvent = nitrobenzene, MW power = 300 W, time = 10 min.

Table 2
Effect of catalyst loadings on the hydroquinone conversion and product selectivity.[a]

Loading (g)	Conversion (%)	2-TBHQ (%)	2,6-DTBHQ (%)	Others[b] (%)
0.05	45.2	98.6	0	1.4
0.10	88.0	93.1	4.0	2.9
0.20	96.0	85.4	7.6	7.0

[a] Reaction temperature = 150 °C, HQ:MTBE = 1:1, solvent = nitrobenzene, MW power = 300 W, time = 8 min.
[b] 4-*tert*-Butoxyphenol, 2,5-di-*tert*-butylhydroquinone.

the presence of low amount of MTBE and the use of mild Brönsted acid catalyst.

3.2.2. Effect of temperature

The effect of temperature on *tert*-butylation reaction was investigated at 135, 150 and 165 °C (Fig. 8A). At 135 °C, 100% selectivity to 2-*tert*-butylhydroquinone was achieved at a 58% conversion level. As expected, the conversion rate increased steadily as the temperature was raised from 135 to 165 °C. However, higher temperature under microwave irradiation led to lower selectivity to 2-*tert*-butylhydroquinone (Fig. 8B). Based on the obtained results, the optimum catalytic performance (best conversion and selectivity to 2-*tert*-butylhydroquinone) was achieved at 150 °C.

3.2.3. Effect of catalyst loading

The catalytic performance is also influenced by the catalyst loading. In the present study, the SO_3H-MCM-41 amount was varied within the 0.05–0.20 g range and the catalytic results are shown in Table 2. After a similar reaction time (8 min), the reactant conversion increased with the catalyst amount. This can be explained by an increase in the number of Brönsted acid sites. Beyond 0.2 g, the catalytic conversion was found to be almost constant with decreasing the selective yield to 2-*tert*-butylhydroquinone.

3.2.4. Effect of mole ratio of reactants

The mole ratio of hydroquinone to MTBE was tuned from 1:1 to 1:6 with 0.1 g of catalyst at 150 °C and the results obtained after similar reaction times (8 min) are summarized in Table 3. This study reveals that the hydroquinone conversion is enhanced with an increase in the MTBE concentration. The conversion increment thus indicates a positive reaction order with respect to MTBE. The higher its concentration, the higher is the chance for MTBE to react with hydroquinone in the presence of SO_3H-MCM-41 to yield the products. An increase in the molar ratio of hydroquinone:MTBE from 1:3 to 1:6, however, leads to a decrease in the selectivity to the desired product (monosubstituted 2-*tert*-butylhydroquinone) and to a slightly increased formation of disubstituted 2,6-di-*tert*-butylhydroquinone byproduct. As expected, high probability of multi-substitutions at hydroquinone is enhanced when MTBE is used in large excess, thus increasing the formation of disubstituted and other products.

Table 3
Effect of reactant ratios on the hydroquinone conversion and product selectivity.[a]

HQ:MTBE ratio	Conversion (%)	2-TBHQ (%)	2,6-DTBHQ (%)	Others[b] (%)
1:1	88.0	93.1	4.0	2.9
1:3	92.7	83.1	11.4	5.5
1:6	95.3	75.6	14.3	10.1

[a] Reaction temperature = 150 °C, catalyst loading = 0.10 g, solvent = nitrobenzene, MW power = 300 W, time = 8 min.
[b] 4-*tert*-Butoxyphenol, 2,5-di-*tert*-butylhydroquinone.

3.2.5. Effect of solvents

The effect of solvents on the activity for the hydroquinone *tert*-butylation reaction was investigated. Four solvents with different polarity (E_N^T) and microwave loss factor ($\tan\delta$), namely *n*-hexane ($E_N^T = 0.009$, $\tan\delta = 0.020$), acetonitrile ($E_N^T = 0.460$, $\tan\delta = 0.062$), chlorobenzene ($E_N^T = 0.188$, $\tan\delta = 0.101$) and nitrobenzene ($E_N^T = 0.324$, $\tan\delta = 0.589$) [52,53] were chosen in this study. The results from Table 4 indicate that the microwave loss factor plays a more significant role than the solvent polarity for the catalytic reaction. Nitrobenzene solvent with a high microwave loss factor gives the highest conversion rate and highest yield to 2-*tert*-butylhydroquinone, whereas *n*-hexane with the lowest microwave loss factor shows the lowest conversion rate. This observation can be attributed to the ability of a solvent to convert electromagnetic microwave energy into heat [54]. As the microwave loss factor is getting higher, the efficiency of the solvent to absorb and convert microwave into heat rises. Thus, a reaction medium with a high microwave loss factor value offers better efficient energy absorption and, consequently, leads to a rapid and homogeneous heating providing a faster reactant conversion.

3.2.6. Effect of the catalysts

The effect of various types of catalysts was also investigated in microwave-assisted *tert*-butylation of hydroquinone. The catalytic performances of H_2SO_4, *para*-toluenesulfonic acid (*p*-TSA), SO_3H-MCM-41 and H-AlMCM-41 were compared. The results presented in Table 5 show that homogeneous catalysts such as H_2SO_4 (35 μl, 98%, 0.644 mmol) and *p*-TSA (0.126 g, 0.662 mmol) give rather high hydroquinone conversion (83.8 and 71.4%, respectively) but show rather 'poor' selectivity to 2-*tert*-butylhydroquinone (73.0 and 78.6%, respectively). On the other hand, mesoporous materials such as SO_3H-MCM-41 and H-AlMCM-41 containing weak and mild acidities are beneficial in catalyzing this reaction. More precisely, both heterogeneous catalysts possess practically identical activities, giving comparable hydroquinone conversion (88.0 and 91.6%, respectively). Compared to H-AlMCM-41, SO_3H-MCM-41 obviously presents a better selectivity to 2-*tert*-butylhydroquinone (93.1%). This observation can be correlated with the smaller pore size of SO_3H-MCM-41 generated from the functionalization of APTES and butyl sulfonic acid in comparison with the bare

Table 4
Effect of solvents on the hydroquinone conversion and product selectivity.[a]

Solvents	Dielectric permittivity, ε	Conversion (%)	2-TBHQ (%)	2,6-DTBHQ (%)	Others[b] (%)
n-Hexane	0.020	30.8	100	0	0
Acetonitrile	0.062	42.3	96.5	1.3	2.2
Chlorobenzene	0.101	61.4	95.8	1.2	3.0
Nitrobenzene	0.589	88.0	93.1	4.0	2.9

[a] Reaction temperature = 150 °C, HQ:MTBE = 1:1, catalyst loading = 0.10 g, MW power = 300 W, time = 8 min.
[b] 4-*tert*-Butoxyphenol, 2,5-di-*tert*-butylhydroquinone.

Table 5
Effect of catalysts on the hydroquinone conversion and product selectivity.[a]

Catalysts	Conversion	2-TBHQ	2,6-DTBHQ	Others[g]
H_2SO_4[b]	83.8	73.0	10.6	16.4
p-TSA[c]	71.4	78.6	13.4	8.0
SO_3H-MCM-41[d]	88.0	93.1	4.0	2.9
H-AlMCM-41[e]	91.6	82.2	12.7	5.1
SO_3H-MCM-41[f]	98.2	87.5	9.4	3.1

[a] Reaction temperature = 150 °C, HQ:MTBE = 1:1, solvent = nitrobenzene, MW power = 300 W, time = 8 min.
[b] 97%, loading = 35 μl (0.644 mmol).
[c] *para*-Toluenesulfonic acid monohydrate, loading = 0.126 g (0.662 mmol).
[d] Loading = 0.1 g.
[e] Loading = 0.1 g, SiO_2/Al_2O_3 = 15.
[f] The preparation procedure and sample characterization can be found in the Supplementary Information.
[g] 4-*tert*-Butoxyphenol, 2,5-di-*tert*-butylhydroquinone.

H-AlMCM-41. Thus, the catalytic study suggests that the acid strength and pore size in SO_3H-MCM-41 plays a crucial role for the enhanced *tert*-butylation of hydroquinone under microwave irradiation. Furthermore, the catalytic performance of our SO_3H-MCM-41 catalyst was also compared with the conventional SO_3H-MCM-41 prepared via post synthetic anchoring of 3-(mercaptopropyl)triethoxysilane (MPTES) followed by oxidation with H_2O_2 (the preparation procedure and characterization of this catalyst can be found in Supplementary Information). The results showed that a high conversion (98.2%) was achieved by conventional SO_3H-MCM-41, where a yield of 87.5% of monosubstituted 2-TBHQ and 9.4% of disubstituted 2,6-DTBHQ was obtained, showing that this catalyst is more acidic and stronger than our SO_3H-MCM-41 (Table 5). The different catalytic performance between both catalysts can be explained by the presence of neighboring amine group in our catalyst that perturbs and weakens the acid strength of sulfonic acid (inset of Figure 7), and this weak-to-mild catalyst is highly beneficial for selectively producing monosubstituted Friedel–Crafts product.

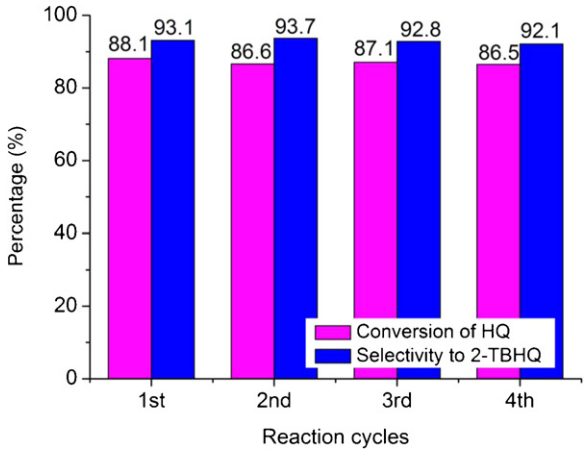

Fig. 9. Product conversion and selectivity from recyclability test. The reaction was carried out at 150 °C, catalyst = 0.1 g, HQ:MTBE = 1:1, solvent = nitrobenzene, MW power = 300 W, time = 10 min.

3.2.7. Leaching and reusability test

Leaching is a major problem for solid catalysts in liquid phase reaction. Therefore, a reusability test for SO_3H-MCM-41 was thus performed and it was found that the reactivity of the recovered SO_3H-MCM-41 was preserved after the second, third and fourth runs (conversion ≈87% and selectivity to 2-*tert*-butylhydroquinone ≈92%, respectively; Fig. 9). This strongly suggests that little to no leaching took place as the sulfonic acid groups are covalently bonded to the mesoporous support. This is consistent with the results obtained from both thermogravimetry and IR spectroscopy analyses.

4. Conclusions

In conclusion, the current work highlights the preparation of covalently anchored sulfonic acid onto the surface of MCM-41 solid via a cyclic sulfate ester ring opening approach. The catalyst was systematically characterized and IR, TG/DTA together with XRD studies evidenced the successful attachment of sulfonic acid group to the walls of MCM-41. The catalytic *tert*-butylation of hydroquinone over SO_3H-MCM-41 under microwave irradiation was also successfully investigated. The solid is catalytically active and shows high selectivity to 2-*tert*-butylhydroquinone. Furthermore, the yield of monosubstituted 2-*tert*-butylhydroquinone was found to increase with temperature and catalyst loading, with stoichiometric MTBE concentration and with the use of solvent with high microwave loss factor ($\tan\delta$). No leaching problem was observed for covalently linked sulfonic acid (—SO_3H) modified MCM-41 and the catalyst can be reused without any reactivity loss. SO_3H-MCM-41 thus offers another environmentally friendly replacement for conventional acidic catalyst.

Acknowledgements

The authors would like to acknowledge FRGS (203/PKIMIA/6711185) and TWAS Research Grants for financial support.

Appendix A. Supplementary data

Supplementary data associated with this article can be found, in the online version, at http://dx.doi.org/10.1016/j.apcata.2012.09.055.

References

[1] G. Rothenberg, Catalysis: Concepts, Green Applications, Wiley-VCH, New York, 2008.
[2] J.H. Clark, Green Chem. 1 (1999) 1–8.
[3] J.H. Clark, Green Chem. 8 (2006) 17–21.
[4] C.T. Kresge, M.E. Leonowicz, W.J. Roth, J.C. Vartuli, J.S. Beck, Nature 359 (1992) 710–712.
[5] W. Zhang, T.R. Pauly, T.J. Pinnavaia, Chem. Mater. 9 (1997) 2491–2498.

[6] E.P. Ng, S. Mintova, Micropor. Mesopor. Mater. 114 (2008) 1–26.
[7] P. Kalita, N.M. Gupta, R. Kumar, J. Catal. 245 (2007) 338–347.
[8] P. Kamala, A. Pandurangan, Catal. Commun. 9 (2008) 605–611.
[9] V.N. Shetti, D. Srinivas, P. Ratnasamy, J. Mol. Catal. A: Chem. 210 (2004) 171–178.
[10] J.R.C. Bispo, A.C. Oliveira, M.L.S. Corrêa, J.L.G. Fierro, S.G. Marchetti, M.C. Rangel, Stud. Surf. Sci. Catal. 142 (2002) 517–524.
[11] P. Selvam, S.E. Dapurkar, Catal. Today 96 (2004) 135–141.
[12] G. Karthikeyan, A. Pandurangan, J. Mol. Catal. A: Chem. 311 (2009) 36–45.
[13] J.C. Juan, J. Zhang, M.A. Yarmo, J. Mol. Catal. A: Chem. 267 (2007) 265–271.
[14] D.P. Sawant, A. Vinu, F. Lefebvre, S.B. Halligudi, J. Mol. Catal. A: Chem. 262 (2007) 98–108.
[15] N.E. Poh, H. Nur, M.N.M. Muhid, H. Hamdan, Catal. Today 114 (2006) 257–262.
[16] E.-P. Ng, H. Nur, K.-L. Wong, M.N.M. Muhid, H. Hamdan, Appl. Catal. A: Gen. 323 (2007) 58–65.
[17] T.V. Kovalchuk, H. Sfihi, A.S. Korchev, A.S. Kovalenko, V.G. Il'in, V.N. Zaitsev, J. Fraissard, J. Phys. Chem. 109 (2005) 13948–13956.
[18] J.-P. Dacquin, H.E. Cross, D.R. Brown, T. Düren, J.J. Williams, A.F. Lee, K. Wilson, Green Chem. 12 (2010) 1383–1391.
[19] J.A. Posada, C.A. Cardona, O. Giraldo, Mater. Chem. Phys. 121 (2010) 215–222.
[20] W.M.V. Rhijn, D.E.D. Vos, B.F. Sels, W.D. Bossaert, P.A. Jacobs, Chem. Commun. (1998) 317–318.
[21] F. Adam, K.M. Hello, M.R.B. Aisha, J. Taiwan Inst. Chem. Eng. 42 (2011) 843–851.
[22] I. Díaz, F. Mohino, E. Sastre, J.P. Pariente, Micropor. Mesopor. Mater. 80 (2005) 33–42.
[23] X. Sheng, J. Gao, L. Han, Y. Xia, W. Sheng, Micropor. Mesopor. Mater. 143 (2011) 73–77.
[24] S. Shylesh, P.P. Samuel, C. Srilakshmi, R. Parischa, A.P. Singh, J. Mol. Catal. A: Chem. 274 (2007) 153–158.
[25] F. Adam, K.M. Hello, T.H. Ali, Appl. Catal. A: Gen. 399 (2011) 42–49.
[26] B. Rác, P. Hegyes, P. Forgo, Á. Molnár, Appl. Catal. A: Gen. 299 (2006) 193–201.
[27] R.V. Hangarge, S.A. Siddiqui, S.R. Shengule, M.S. Shingare, Mendeleev Commun. 12 (2002) 209–210.
[28] L. Guerreiro, I. Fonseca, R.M. -Aranda, A. Ramos, A.B. do Rego, J. Vital, Phosphorus Sulfur Silicon Relat. Elem. 180 (2005) 1485–1486.
[29] M.H. Lim, C.F. Blanford, A. Stein, Chem. Mater. 10 (1998) 467–470.
[30] V.R. Choudhary, V.H. Tillu, V.S. Narkhede, H.B. Borate, R.D. Wakharkar, Catal. Commun. 4 (2003) 449–453.
[31] M. Sharifi, J. Schneider, M. Wark, Micropor. Mesopor. Mater. 151 (2012) 506–510.
[32] H.-Y. Shen, Z.M.A. Judeh, C.B. Ching, Q.-H. Xia, J. Mol. Catal. A: Chem. 212 (2004) 301–308.
[33] A. Sakthivel, S.K. Badamali, P. Selvam, Micropor. Mesopor. Mater. 39 (2000) 457–463.
[34] R.D. O'Brien, Fats and Oils: Formulating and Processing for Applications, 2nd ed., CRC Press, New York, 2004, p. 16.
[35] J. Chen, Evaluation of National Assessments of Intake of Intake Tert-butylhydroquinone (TBHQ), International Programme on Chemical Safety (IPCS), World Health Organization, Geneva, 1999.
[36] X. Wang, K.S.K. Lin, J.C.C. Chan, S. Cheng, J. Phys. Chem. B 109 (2005) 1763–1769.
[37] K. Miyatake, H. Iyotani, K. Yamamoto, E. Tsuchida, Macromolecules 29 (1996) 6969–6971.
[38] R. Langner, G. Zundel, J. Phys. Chem. 99 (1995) 12214–12219.
[39] S. Schmitt, C. Bouteiller, L. Barré, C. Perrio, Chem. Commun. 47 (2011) 11465–11467.
[40] Z. Navatilova, P. Wojtowicz, L. Vaculikova, V. Sugarkova, Acta Geodyn. Geomater. 4 (2007) 59–65.
[41] X. Chen, Y. Li, G. Guang, Z. Dai, W. Fu, Z. Shi, D. Zhang, Y. Xu, S. Feng, Chem. Res. Chin. Univ. 20 (2004) 24–28.
[42] Q. Peng, Y. Yang, Y. Yuan, J. Mol. Catal. A: Chem. 219 (2004) 175–181.
[43] R.I. Kureshy, I. Ahmad, N.H. Khan, S.H.R. Abdi, K. Pathak, R.V. Jasra, J. Catal. 238 (2006) 134–141.
[44] X. Wang, Y.-H. Tseng, J.C.C. Chan, S. Cheng, J. Catal. 233 (2005) 266–275.
[45] C.R. Martins, G. Rugger, M.A.D. Paoli, J. Braz. Chem. Soc. 14 (2003) 797–802.
[46] J.C. Groen, L.A.A. Peffer, J.P. Ramirez, Micropor. Mesopor. Mater. 60 (2003) 1–17.
[47] E.B. Wilson, Physiol. Rev. 45 (1934) 706–714.
[48] A. Vimont, J.C. Lavalley, A. Sahibed-Dine, C.O. Arean, M.R. Delgado, M. Daturi, J. Phys. Chem. B 109 (2005) 9656–9664.
[49] G. Leofanti, M. Padovan, G. Tozzola, B. Venturelli, Catal. Today 41 (1998) 207–219.
[50] R.W. Stevens, S.S.C. Chuang, B.H. Davis, Appl. Catal. A: Gen. 252 (2003) 57–74.
[51] A. Zecchina, L. Marchese, S. Bordiga, C. Pazè, E. Gianotti, J. Phys. Chem. B 101 (1997) 10128–10135.
[52] B.L. Hayes, Microwave Synthesis: Chemistry at the Speed of Light, CEM Publishing, Matthews, NC, 2002.
[53] J. Zou, Q. Yu, Z. Shang, J. Chem. Soc., Perkin Trans. 2 (2001) 1439–1443.
[54] C.O. Kappe, Angew. Chem. Int. Ed. 43 (2004) 6250–6284.